Giant rectification in strongly-interacting boundary-driven tilted systems

Juan José Mendoza-Arenas[1, *] and Stephen R. Clark[1, †]

[1] *H. H. Wills Physics Laboratory, University of Bristol, Bristol, BS8 1TL, United Kingdom*

(Dated: September 26, 2022)

Correlated quantum systems feature a wide range of nontrivial effects emerging from interactions between their constituting particles. In nonequilibrium scenarios, these manifest in phenomena such as many-body insulating states and anomalous scaling laws of currents of conserved quantities, crucial for applications in quantum circuit technologies. In this work we propose a giant rectification scheme based on the asymmetric interplay between strong particle interactions and a tilted potential, each of which induces an insulating state on their own. While for reverse bias both cooperate and induce a strengthened insulator with exponentially suppressed current, for forward conduction they compete and, as a result, generate current resonances; this leads to a rectification coefficient of many orders of magnitude. We uncover the mechanism underlying these resonances as enhanced coherences between energy eigenstates occurring at avoid crossing in the system's bulk energy spectrum. Our proposal paves the way for implementing a perfect diode in currently-available quantum simulation platforms.

INTRODUCTION

Due to their vast and exciting phenomenology, as well as the rapid advances on their control protocols, many-body quantum systems have become key ingredients for the development of novel technologies at the nanoscale. In particular, in nonequilibrium regimes such systems feature properties which make them strongly appealing for applications in quantum circuits [1–4]. This has been exemplified in several platforms where tunable transport of particles or heat can be induced and characterized, including setups based on electronic devices such as molecular electronics [5] and quantum dots [6, 7], or on quantum simulators such as cold atoms [8, 9] and superconducting qubits [10, 11].

In parallel to these seminal experimental advances, there have been numerous recent theoretical proposals to use quantum systems of interacting particles as different types of circuit elements that efficiently perform specific tasks. This includes autonomous quantum thermal machines [12–14], transistors [15, 16], magnetoresistors [17], and a quantum analogue of the Wheatstone bridge [18]. Much attention in this area has been directed towards quantum diodes [19–30]. There, spatial asymmetries and non-linearities are engineered together to allow transport in one direction under a chemical potential, magnetic or thermal bias, and to suppress it in the opposite direction when the bias is inverted. These efforts include the proposal of giant rectification setups [20, 25–28], which rely on complicated geometries and potential landscapes to induce rectification coefficients of several orders of magnitude using finely-tuned parameters.

Here we put forward a rectification scheme which naturally emerges over a broad range of parameters in tilted interacting quantum lattices. These systems have been

the object of intense recent research as they feature disorder-free (Stark) many-body localization (MBL) [31–35], quantum scars [36, 37], and counter-intuitive phenomena such as time crystals [38] and transport opposite to an applied electric field [39]. Moreover, they have been implemented experimentally in several quantum simulation platforms [40–44], making them attainable for state-of-the-art applications in quantum technologies. Neither the spatial asymmetry of the tilted onsite-potential nor the non-linearity of inter-particle interactions can on their own induce rectification. However, the ability to simultaneously implement both ingredients in such platforms opens the possibility of rectification. Here we unveil the underlying mechanism of this interaction-tilt interplay and show how the vastly differing transport properties [45] with the direction of bias give rise to giant rectification even with moderate interactions.

RESULTS

Giant rectification scheme. Our quantum diode is based on a boundary-driven configuration, which can be biased from right to left (*reverse driving*) or left to right (*forward driving*). For reverse driving, sketched in Fig. 1a, both interactions and tilt each support on their own the formation of a high-energy current-blocking particle domain at the right boundary. When interactions and tilt coexist they thus cooperate to induce a high-energy state with an enhanced insulating nature. For forward driving, depicted in Fig. 1b, both strong interactions and tilt favour on their own the formation of an insulating domain at the left boundary. For interactions alone this state remains high-energy, while for the tilt alone it is low-energy (see Fig. 1c). By being located at opposite ends of the energy spectrum interactions and tilt now conflict with each other when they coexist. When both are of similar order, this competition breaks the domains and thus allows particle conduction. This forward-reverse transport asymmetry makes the system behave as

* juanjose.mendozaarenas@bristol.ac.uk
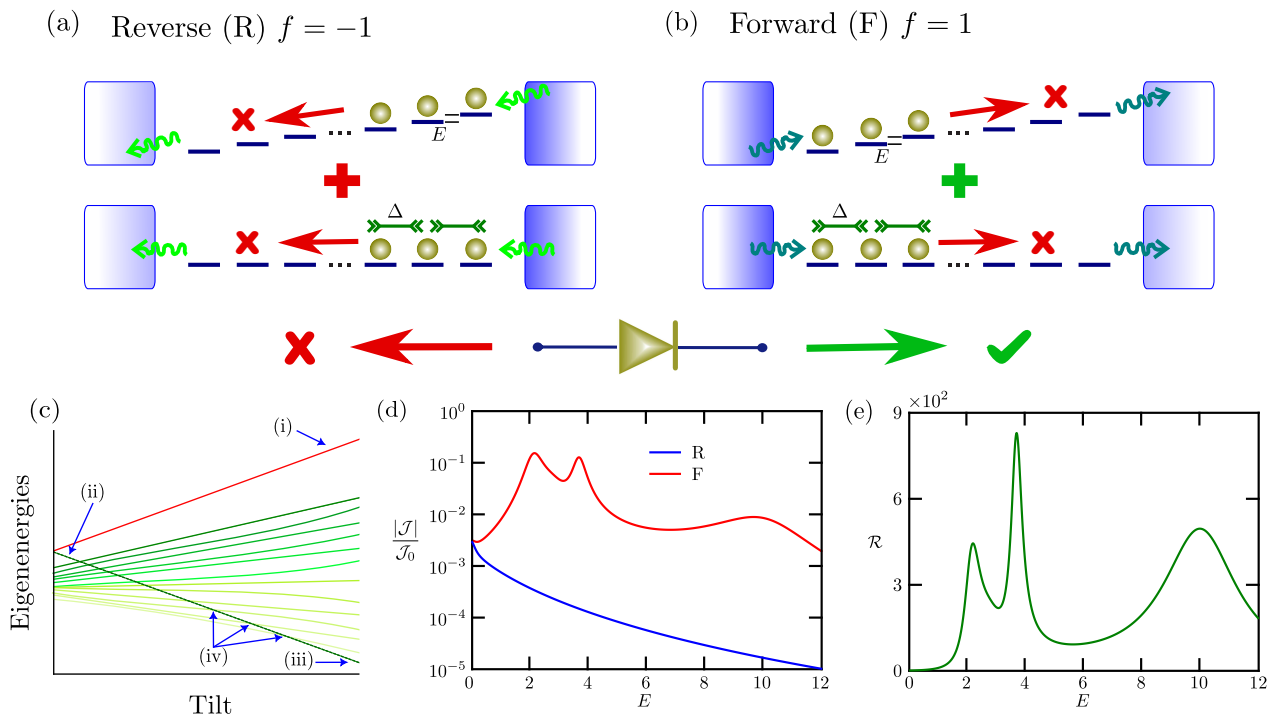† stephen.clark@bristol.ac.uk

FIG. 1. Giant rectification in tilted strongly-interacting lattice. **a** For reverse transport, particles are mostly injected from a reservoir on the right boundary of the system, and mostly ejected to a reservoir on the left. For interactions or tilt alone, the resulting state is of high-energy, due to the adjacency of particles in the former case, or due to the particles filling the top of the potential in the latter. An enhanced insulator is induced when both coexist. **b** For forward transport, particles flow from the left to the right reservoir. The tilted noninteracting state is of low energy as particles now fill the bottom of the potential. Thus tilt now competes with interactions, which favors conduction. **c** Sketch of the eigenstructure of a tilted interacting system. (i) High-energy insulating eigenstate preferentially populated by reverse bias. (ii) High-energy insulating eigenstate preferentially populated by forward bias and dominant interactions. (iii) Low-energy insulating eigenstate preferentially populated by forward bias and very large tilt. (iv) The path from the interaction- to the tilt-dominated insulator, indicated by the dashed line, features avoided crossings at intermediate regimes where occupation probability is transferred between eigenstates, enhancing the transport. **d** Forward (F) and reverse (R) particle currents in a lattice of $N = 4$ and $\Delta = 5$ as a function of the tilt. Currents have been rescaled by the maximum current $\mathcal{J}_0$ obtained with the same driving for a noninteracting homogeneous system (see Supplementary Methods). **e** The corresponding rectification coefficient $\mathcal{R}$.

a quantum diode.

To unveil this phenomenon we consider a simple generic model of interacting particles: a one-dimensional lattice of spinless fermions in a tilted potential. The Hamiltonian for N sites is

$$H = \sum_{j=1}^{N-1} \left[\frac{J}{2} \left(c_j^\dagger c_{j+1} + \text{H.c.} \right) + \Delta \left(n_j - \frac{1}{2} \right) \left(n_{j+1} - \frac{1}{2} \right) \right]$$
$$+ \sum_{j=1}^{N} \left(\mu + \frac{E}{2} j \right) \left(n_j - \frac{1}{2} \right), \quad (1)$$

where $c_j^\dagger$ (c_j) creates (annihilates) a fermion on site j, $n_j = c_j^\dagger c_j$ is the corresponding particle number operator, J is the hopping amplitude (we take $J = 1$ to set the energy scale), Δ is the nearest-neighbor density-density interaction, and μ is the diode's chemical potential. We take the tilt strength $E > 0$ so the potential always increases from left to right. For the noninteracting case

$\Delta = 0$, this model shows Wannier-Stark localization [46]. Furthermore, it was recently discovered that for strong enough tilt the interacting model still features nonergodic behavior in the absence of disorder, an effect known as Stark MBL [31, 32].

To drive the system to a nonequilibrium state, we incorporate reservoirs with differing chemical potentials at its boundaries. We assume a weak coupling to the system (Born approximation), high-temperature memory-less reservoirs (Markov approximation), and that the bandwidths of the reservoirs are much larger than those of the system, which leads to frequency-independent system-reservoir interactions (wide-band limit) [47]. Tracing out the reservoir degrees of freedom leads to a Lindblad master equation for the reduced density matrix ρ of the system [48],

$$\frac{d\rho}{dt} = -i[H, \rho] + \sum_k \mathcal{L}_k(\rho), \quad (2)$$
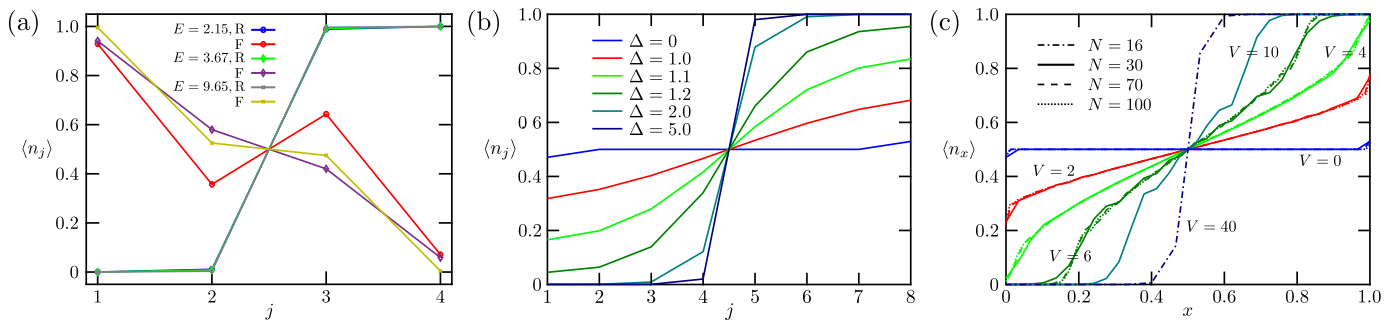
FIG. 2. Formation of particle domains. **a** Site population $\langle n_j \rangle$ for $N = 4$, $\Delta = 5$ and the resonant tilt values, for forward and reverse driving. **b** Site population $\langle n_j \rangle$ for a lattice of $N = 8$, $E = 0$ and different interactions Δ for reverse driving. **c** Site population $\langle n_x \rangle$ for $\Delta = 0$, different system sizes and rescaled tilt V, with rescaled position $x = j/N \in [0, 1]$.

with the dissipative superoperators $\mathcal{L}_k(\rho)$ defined by jump operators L_k as

$$\mathcal{L}_k(\rho) = L_k \rho L_k^\dagger - \frac{1}{2}\{L_k^\dagger L_k, \rho\}. \qquad (3)$$

The driving is induced by boundary operators $L_{1,N}^+ = \sqrt{\Gamma(1 \pm f)/8}\, c_{1,N}^\dagger$ and $L_{1,N}^- = \sqrt{\Gamma(1 \mp f)/8}\, c_{1,N}$, where Γ is the coupling strength (taken as $\Gamma = 1$) and the driving parameter $-1 \le f \le 1$ establishes the bias [4, 49, 50]. Namely, when $f > 0$, fermions are mostly created on site 1 and mostly annihilated on site N giving forward driving, while inverting the sign of f gives reverse driving. The particle current corresponds to the expectation value of the operator

$$\mathcal{J}_j = i\frac{J}{2}\left(c_j^\dagger c_{j+1} - c_{j+1}^\dagger c_j\right), \qquad j = 1, \ldots, N-1, \quad (4)$$

which directly arises from the particle number continuity equation [4]. We focus on the transport properties of the nonequilibrium steady state (NESS), where the current across the system is homogeneous, i.e. $\langle \mathcal{J}_j \rangle = \mathcal{J}$. In addition, we set $|f| = 1$ to consider maximal forward/reverse driving, and take $\mu = -E(N+1)/4$ so the system features charge conjugation and parity (CP) symmetry. This choice will help make the rectification mechanism transparent. Nonetheless, under the assumed wide-band limit for the driving, the transport is independent of μ [51] (see Methods).

This simple nonequilibrium scenario allows us to observe large rectification even for very small lattices. For instance, in Fig. 1d we illustrate the widely differing response of a system with $N = 4$ and $\Delta = 5$ when inverting the direction of the bias. For reverse driving of fermions down the tilted potential, the current decays rapidly and monotonically with E. On the other hand, for forward driving of fermions up the potential, the current features much larger values at well-defined resonances with E. As shown in Fig. 1e, this leads to rectification coefficients of up to $O(10^3)$, a value that can be vastly enhanced in longer chains (see Fig. 4).

These properties are intimately linked to the presence or absence of a particular distribution of fermions across the system, as depicted in Fig. 2a. For reverse driving, the particles are pinned to the right boundary forming a domain half the size of the lattice, leaving the left half essentially unoccupied. The domain Pauli blocks more fermions from entering the system, resulting in an insulating state. For forward bias near the resonant values of E, the population profiles do not feature this constraint, so particles are allowed to move across the lattice.

Reverse driving insulating NESS. Domain formation is a common feature induced by strong interactions and tilt on their own, as depicted in Figs. 2b where $E = 0$ and 2c where $\Delta = 0$. In both these scenarios there is no rectification; transport for forward and reverse drivings are identical up to a direction inversion, so we focus our attention to the latter.

For strongly-interacting homogeneous ($E = 0$) systems the insulating domain-like NESS is a well-known phenomenon [4, 49, 50, 52], reproduced in Fig. 2b with exact diagonalization calculations for small lattices (see Methods). The system features a flat profile in the noninteracting limit, typical of ballistic transport. As Δ increases so does the slope of the profile, until reaching extreme population values at the boundaries for $\Delta \gtrsim 1$. Increasing Δ even further results in the creation of the particle domain.

In contrast noninteracting ($\Delta = 0$) boundary-driven tilted systems have received much less attention [53] and their manifestation of localization has remained unexplored. We perform such an analysis obtaining exactly the site populations $\langle n_j \rangle$ and particle current $\mathcal{J}$ for large systems by reducing the Lindblad master equation (2) to a set of linear equations (see Methods). We use a rescaled tilt $V = EN$, to keep the on-site energy difference between boundaries approximately constant. This way the density profiles of different system sizes collapse for each V, evidencing the emergence of domains for small lattices and large tilt, as well as for long lattices and low tilt. In addition, for large systems the current decays exponen-
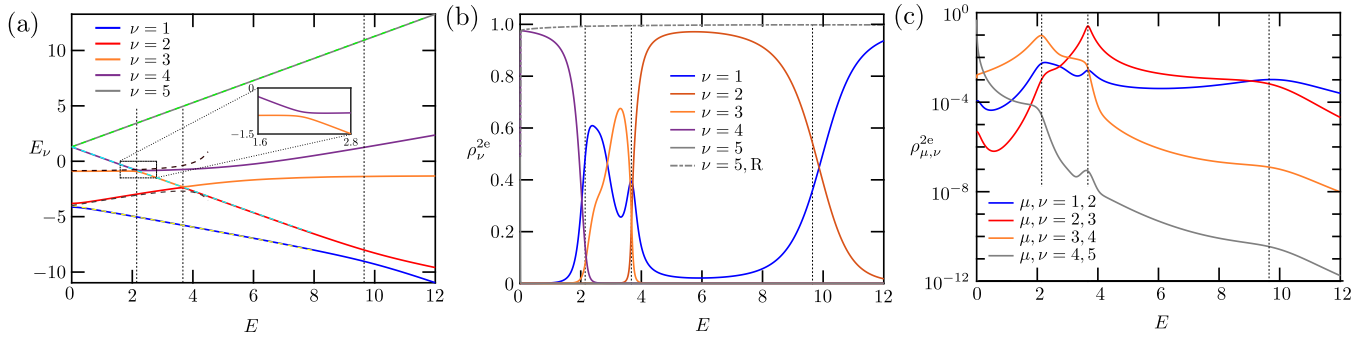
FIG. 3. Transport resonance mechanism in interacting tilted lattice of $N = 4$ and $\Delta = 5$, illustrated in the "even" CP symmetry sector of $n = 2$ filling (sector $s = 2\mathrm{e}$). In all panels, the dotted vertical lines indicate the location of the forward current resonances. **a** Eigenenergies E_ν as a function of the tilt E. For low tilts, the eigenstate $\nu = 4$ corresponds to the corrected left domain state. The inset amplifies the first avoided crossing. The dashed lines correspond to second order perturbative calculations of the eigenenergies (see Supplementary Methods). **b** Probabilities $\rho_\nu^{2\mathrm{e}}$ of eigenstates ν on the NESS. The line of $\nu = 5, \mathrm{R}$ corresponds to the highest energy eigenstate and reverse transport; all the others are for forward driving. Also note that the curve of $\nu = 1$ is peaked at the first two resonances, even though it is not involved in an avoided crossing. This is because it corresponds to a perturbative correction of $|1010\rangle$ (see Supplementary Methods), which is strongly coupled to the $f = 1$ driving. **c** Coherences $\rho_{\mu,\nu}^{2\mathrm{e}}$ of pairs of eigenstates μ, ν for forward transport. At the avoided crossing of eigenstates μ and $\mu + 1$, $\rho_{\mu,\mu+1}^{2\mathrm{e}}$ is maximal, which breaks the insulating nature of the NESS. Also, when getting away from avoided crossings, the NESS is again mostly described by a single eigenstate suppressing transport.

tial with N and V (See Supplementary Discussion).

While the physical origin of the interaction- and tilt-induced insulating states is different, they share the same underlying mechanism that remains applicable for tilted interacting lattices. Specifically, they arise from the interplay between the gapped eigenstructure of the system and the maximal driving. For small hopping $J \ll \Delta$ or E, the highest energy eigenstate $|\Psi_n^D\rangle$ of each n particle sector (e.g. eigenstate $\nu = 5$ of Fig. 3a) corresponds to a perturbative correction to the configuration state $|00\ldots0_{N-n}11\ldots1_n\rangle$ in which all n particles form a domain pinned to the right. The energy gap between this eigenstate and the rest, which increases with Δ and E, ensures that the amplitudes of configuration states in $|\Psi_n^D\rangle$ that couple to the $f = -1$ driving (where a particle can be injected at site N or ejected at site 1) are exponentially suppressed (see Supplementary Methods). Thus the eigenstates $|\Psi_n^D\rangle$ become exponentially close to obeying $\sum_k \mathcal{L}_k(|\Psi_n^D\rangle\langle\Psi_n^D|) = 0$, making them *dark states* of the driving. The overall NESS density matrix ρ of the system is very well captured by an analytical Ansatz built from a statistical mixture of these darks states (see Eq. (8) of Methods and Supplementary Discussion). From this, we show that ρ is strongly dominated by the contribution $|\Psi_n^D\rangle\langle\Psi_n^D|$ with $n = N/2$, corresponding to a state with occupied and empty domains of equal size (e.g. near unit probability for state $\nu = 5$ for reverse driving in Fig. 3b). These results directly lead to the insulating NESSs of equal empty and occupied domains for systems with strong interactions [50], tilt or both, whose currents monotonically and exponentially decrease as they increase.

Forward driving resonances. Next we focus on the forward driving setup with $f = 1$. Here, strong interactions and tilt on their own would favor a NESS largely dominated by perturbative corrections to the left domain $|11\ldots1_{\frac{N}{2}}00\ldots0_{\frac{N}{2}}\rangle$. However, this configuration is the highest energy state of the $n = N/2$ particle number sector (degenerate with the right domain) for an interaction-dominated scenario, while it is the lowest energy state for a strongly tilted lattice. Thus, increasing Δ raises the energy of this state, while increasing E lowers it. For instance, fixing Δ and sweeping through E (as in Fig. Fig. 3a) closes the energy gap from the initial NESS dark state, eventually forcing it to cross through the bulk spectrum of the system (see sketch in Fig. 1c). As a result, current resonances are induced. This effect is cleanly illustrated by the half-filled even CP symmetric sector with the same parameters of Fig. 1d as shown in Fig. 3a. Crucially, since all the eigenstates have the same symmetry, the no-crossing theorem [54] ensures that only avoided crossings occur. Their location accurately pinpoints the current resonances.

To understand the role of the avoided crossings we evaluate the contributions to the particle current in the energy eigenbasis. Since there are no coherences between different symmetry sectors, the current is given by $\mathcal{J} = \sum_s \sum_{\mu_s, \nu_s} \rho_{\mu_s, \nu_s}^s \mathcal{J}_{\nu_s, \mu_s}^s(q)$, where s sums over all the sectors, $\rho_{\mu_s, \nu_s}^s = \langle \mu_s | \rho | \nu_s \rangle$ is the coherence between eigenstates $|\mu_s\rangle$ and $|\nu_s\rangle$ of sector s, and $J_{\nu_s, \mu_s}^s(q) = \langle \nu_s | \mathcal{J}_q | \mu_s \rangle$ is the corresponding current matrix element evaluated on site q. From the probabilities $\rho_{\nu_s}^s = \rho_{\nu_s, \nu_s}^s$ and coherences ρ_{μ_s, ν_s}^s, shown in Figs. 3b and 3c respectively, the following picture emerges. For very low tilts, the NESS is solely dominated by the high-energy left domain-like
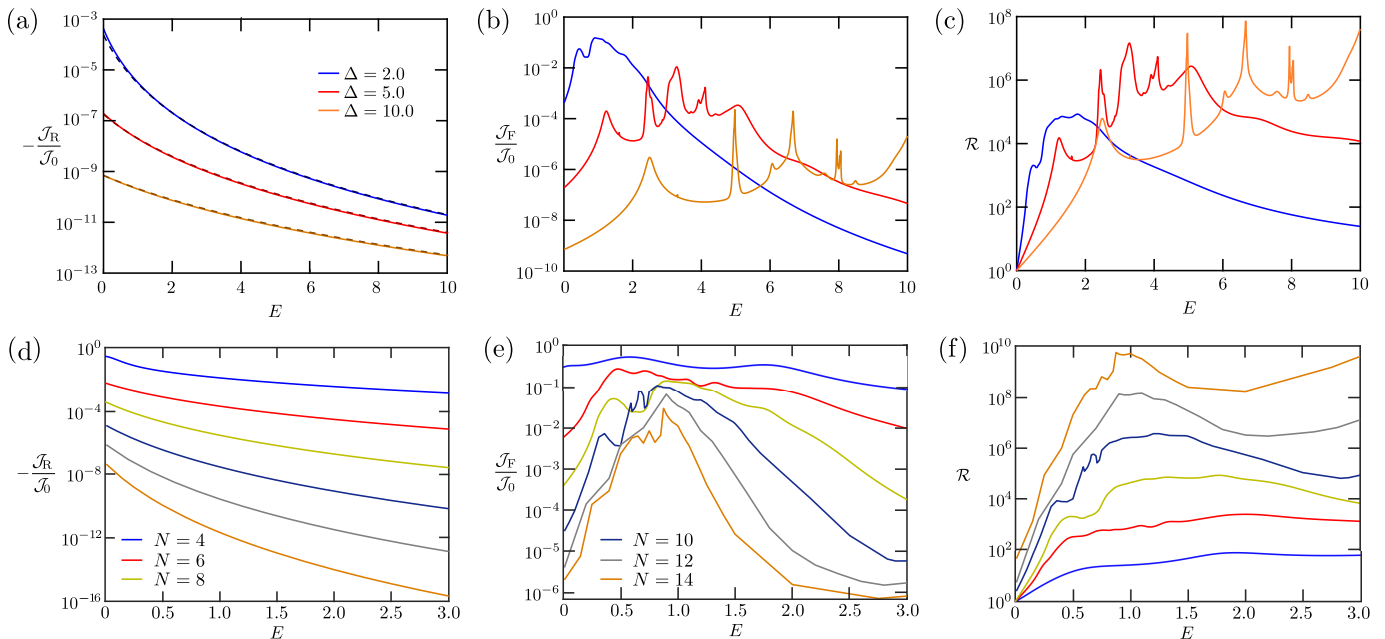
FIG. 4. Transport and rectification in larger interacting tilted systems. **a** Reverse particle current $\mathcal{J}_R$ as a function of tilt for $N = 8$ and different interaction strengths. The solid lines correspond to exact diagonalization results, and the darker dashed lines to currents obtained from our analytical Ansatz (see Methods). **b** Exact forward particle current $\mathcal{J}_F$ for the same parameters. **c** Corresponding rectification coefficient $\mathcal{R}$. **d** Reverse particle current $\mathcal{J}_R$ as a function of tilt for $\Delta = 2$ and different system sizes. **e** Forward particle current $\mathcal{J}_F$ for the same parameters. **f** Corresponding rectification coefficient $\mathcal{R}$. The legends of system sizes spread over **d** and **e** apply to the three bottom panels. Also, the currents have been rescaled by the maximal current $\mathcal{J}_0$ obtained with the same driving for a noninteracting homogeneous system (see Supplementary Methods).

state, evidenced by its large probability. This eigenstate has an energy $\sim \frac{1}{4}\left[\Delta(N-3)-En(N-n)\right] + \mathcal{O}(J^2)$ to lowest perturbative order (see Supplementary Methods), so as E increases it dives down towards the lower eigenenergies which have a weaker dependence on the tilt. As it approaches another eigenstate they mix and probability is transferred from the higher to the lower energy states. Thus, in the proximity of the avoided crossing the Hamiltonian no longer supports an eigenstate that is dark to the $f = 1$ driving. This allows large coherences to develop, enhancing the current. Further avoided crossings occur for even larger E, with lower eigenstates also getting populated. Eventually for very large E the whole spectrum is crossed and the lowest-energy eigenstate $\nu = 1$ inherits the dominant role on the NESS. This leads again to an insulating left domain-like dark state, but now induced by the strong tilt.

The combination of this resonant behavior with the enhanced insulating state of reverse driving results in sizable rectification coefficients $\mathcal{R} = -\mathcal{J}_F/\mathcal{J}_R$ even for the small chain of the example (see Fig. 1e). Crucially, rectification becomes more substantial and more robustly achievable for larger system sizes N. The enhancement in the maximum $\mathcal{R}$ with N follows from the differing current scaling of reverse and forward drivings. Namely $\mathcal{J}_R \sim \exp(-N)$, characteristic of an insulator, while at a resonance we expect $\mathcal{J}_F \sim N^{-\alpha}$ with some exponent

$\alpha > 0$ characteristic of a conductor. As shown in Fig. 4c, already for $N = 8$ with $\Delta = 5$ we find coefficients of up to $\mathcal{O}(10^7)$ compared to $\mathcal{O}(10^3)$ for $N = 4$. In addition, $\mathcal{R}$ is further enhanced by particle interactions. As depicted in Figs. 4a-c, while increasing Δ diminishes both reverse and forward currents, the former decrease is more prominent and thus their ratio features even higher resonances.

While in small systems achieving the maximum $\mathcal{R}$ requires fine-tuning of E to locate a resonance, for larger N this constraint is rapidly removed due to the exponentially increasing number of eigenstates crossed within the bulk of the spectrum. As a result the rectification is broadened over the many-body bandwidth of the chain. Moreover, the favourable scaling with N means that giant rectification can be achieved with a reduced interaction strength. To evidence these effects, using the insulating Ansatz and tensor network simulations (see Methods) we calculated reverse and forward currents for $\Delta = 2$ and systems of $N > 8$, shown in Figs. 4d and 4e respectively. From these we find $\mathcal{R} \sim \mathcal{O}(10^9)$ over a range of E, as seen in Fig. 4f. This establishes larger rectification coefficients than those previously obtained for different types of non-homogeneous lattices [20, 25–28], with a more intuitive and easily implementable setup [41–44].

DISCUSSION

We have proposed a giant rectification scheme in correlated quantum systems, based on the natural asymmetry between forward and reverse transport in tilted interacting lattices. In our protocol, particles get locked into an insulating domain NESS when attempting to travel down the tilted potential (reverse bias). On the other hand, they propagate uphill resonantly as avoided crossings in the spectrum are approached (forward bias). Our calculations show rectification coefficients of up to $O(10^9)$ for small chains, a number that can be pushed even further without fine tuning and at moderate interaction strengths by considering larger systems.

We emphasize that most of the reported rectification peaks are associated to sizeable values of the forward particle currents. This is evidenced in Figs. 1 and 4 by rescaling $\mathcal{J}$ with the maximal current $\mathcal{J}_0$ achievable under the same driving scheme for a noninteracting lattice with no tilt, which is a well-known size-independent ballistic current (see Supplementary Methods). This way it is clear that at the resonances the system is truly conducting in the forward direction while it is insulating in reverse bias. Thus the observed giant rectification is not an artifact of dividing two very small currents associated to insulating states.

Our results pave the way for developing different types of giant rectification protocols (e.g. of spin, charge or heat) in a variety of driving schemes, including finite temperature reservoirs, and magnetic or thermal biases. For this purpose, recent approaches for accurately simulating more realistic reservoirs, even when they are strongly coupled to the system, might be exploited [12, 55–57]. Furthermore, our proposal could be realized with existing quantum simulators. On the one hand, several experiments have implemented trapped ion [40], cold-atom [41–43] and superconducting qubit [44] setups with similar tilt and/or interactions to those used in the present work, and even in larger systems. In addition, exploiting boundary-driven architectures in cold-atom platforms [9, 19, 58] or reservoir engineering for irreversible particle injection in superconducting circuits [59], similar versions of our diode could be incorporated in state-of-the-art nanoscale quantum circuits.

METHODS

Exact solution of noninteracting model. The relevant observables for our transport analysis can be obtained for large systems with $\Delta = 0$. For this we propose the Ansatz for the density matrix [51, 60]

$$\rho = \frac{1}{2^N} I + \sum_{k=1}^{N} 2a_k \left(n_k - \frac{1}{2} \right)$$
$$+ \sum_{l=2}^{N} \sum_{k=1}^{N-l+1} b_k^{(l)} B_k^{(l)} + \sum_{l=2}^{N} \sum_{k=1}^{N-l+1} h_k^{(l)} H_k^{(l)} + \cdots \tag{5}$$

where we define the $l-$site operators

$$B_k^{(l)} = -2i \left(c_j^\dagger c_{j+l-1} - c_{j+l-1}^\dagger c_j \right)$$
$$H_k^{(l)} = 2 \left(c_j^\dagger c_{j+l-1} + c_{j+l-1}^\dagger c_j \right), \tag{6}$$

which correspond to generalized current and energy density operators respectively; in particular, $B_k^{(2)} = -4\mathcal{J}_k$. Even though this is a first-order expansion in f [51, 60], it leads to an exact solution of the parameters $a_k = \langle 2n_k - 1 \rangle$, $b_k^{(l)} = \langle B_k^{(l)} \rangle / 2$ and $h_k^{(l)} = \langle H_k^{(l)} \rangle / 2$. For this, the Ansatz (5) in inserted into the master equation (2) with the stationary condition $d\rho/dt = 0$, which results in a closed set of linear equations for the parameters when grouping the coefficients in front of each operator (see Supplementary Methods). Notably, through this linear set it is straightforward to link the boundary population and the current, since from the coefficients in front of $2n_1 - 1$ we get

$$a_1 + \frac{4b^{(2)}}{\Gamma} = f, \qquad \text{with } b^{(2)} = b_k^{(2)} \text{ homogeneous.} \quad (7)$$

Exploiting the symmetric boundary driving, it is found that several coefficients are equal to their counterpart from the other half of the lattice (e.g., $a_k = a_{N-k+1}$, so the population profile is symmetric around 0.5) or zero (e.g., $a_{\frac{N+1}{2}} = 0$ for N odd). This leads to a system of $\frac{N^2}{2} + 1$ unknowns for N even and $\frac{(N-1)^2}{2} + 1$ unknowns for N odd, which can be solved with standard linear algebra packages for lattices of several hundreds of sites. Analytical solutions for small systems are provided in the Supplementary Discussion.

Calculation of transport properties. The transport properties of small lattices ($N \leq 8$) was obtained exactly by diagonalizing the full Lindblad superoperator, written as a $4^N \times 4^N$ matrix. The NESS is the eigenstate with zero eigenvalue, reshaped as the $2^N \times 2^N$ density matrix ρ. For larger systems and forward transport, we describe ρ as a matrix product state [61], and obtain the particle current using the time evolving block decimation method [62, 63] implemented with the Tensor Network Theory (TNT) library [64, 65]. Here, the evolution of an arbitrary state should be simulated until the current becomes homogeneous, which indicates convergence. However, strong tilts and interactions commonly result in a very slow approach to the NESS, making it impractical. Thus, in such cases we focused on converging expectation values on the first site only. This shortcut allowed us to

reproduce very well the current of small lattices, so we extended its application to longer chains.

For $N > 8$ and reverse transport, where even the previous shortcut is not enough due to exponentially slow convergence to the NESS [49, 50], we calculate the current from the analytical Ansatz for insulating states. This is given by (see Supplementary Methods)

$$\rho_{\mathrm{Dom}} = \sum_{n=0}^{N} p_n |\Psi_n^D\rangle\langle\Psi_n^D|, \qquad \sum_{n=0}^{N} p_n = 1, \qquad (8)$$

which captures remarkably well the particle density profile. The current is calculated from the population of the first site, as Eq. (7) is generally valid [4, 52]. Since the considered system sizes can have very low currents $\mathcal{J} < 10^{-15}$, exact calculations from this Ansatz were performed in MATLAB using the Variable-precision arithmetic (vpa) function to take 32 digits of precision.

CP symmetry of tilted interacting model. Hamiltonian (1) is invariant under simultaneous charge conjugation and center-reflection operations, e.g. $U n_j U^\dagger = 1 - n_{N-j+1}$ for the CP symmetry operator U. Also, since $U^2 = I$, its eigenvalues are ± 1, corresponding to even and odd symmetry. However, only at half filling U commutes with the total particle number operator $\tilde{N} = \sum_j n_j$, since $U\tilde{N}U^\dagger = N - \tilde{N}$. Thus, only in this case we can consider particle number conservation and CP symmetry simultaneously. This property is used to build the Hamiltonian of the even CP half-filled symmetry sector (see Supplementary Methods) whose energy eigenspectrum features the avoided crossings that coincide with the forward current resonances (see Fig. 3a).

Crucially, this does not mean that our giant rectification mechanism relies on the presence of CP symmetry. In fact, the particle transport remains identical when this symmetry is broken by taking $\mu \neq -E(N+1)/4$. This occurs because within the assumed wide-band limit, the energy gap between different particle number sectors (controlled by μ) is irrelevant. Only the energy differences between eigenstates within each sector, which are independent of μ, are important for our device. The CP symmetry just allows us to isolate even and odd eigenstates, transparently evidencing the connection between the avoided crossings and current resonances.

In light of this discussion, also note that forward particle transport is identical (up to a direction change) to reverse transport with inverted tilt $-E$.

[1] Giuliano Benenti, Giulio Casati, Keiji Saito, and Robert S. Whitney. Fundamental aspects of steady-state conversion of heat to work at the nanoscale. *Phys. Rep.*, 694:1–124, 2017. Fundamental aspects of steady-state conversion of heat to work at the nanoscale.

[2] B. Bertini, F. Heidrich-Meisner, C. Karrasch, T. Prosen, R. Steinigeweg, and M. Žnidarič. Finite-temperature transport in one-dimensional quantum lattice models. *Rev. Mod. Phys.*, 93:025003, May 2021.

[3] Jukka P. Pekola and Bayan Karimi. Colloquium: Quantum heat transport in condensed matter systems. *Rev. Mod. Phys.*, 93:041001, Oct 2021.

[4] Gabriel T. Landi, Dario Poletti, and Gernot Schaller. Non-equilibrium boundary driven quantum systems: models, methods and properties. *arXiv*, arXiv:2104.14350v2:1, 2022.

[5] N. Xin, J. Guan, C. Zhou, X. Chen, C. Gu, Y. Li, M. A. Ratner, A. Nitzan, J. F. Stoddart, and X. Guo. Concepts in the design and engineering of single-molecule electronic devices. *Nat. Rev. Phys.*, 1:211, 2019.

[6] M. Josefsson, A. Svilans, A. M. Burke, E. A. Hoffmann, S. Fahlvik, C. Thelander, M. Leijnse, and H. Linke. A quantum-dot heat engine operating close to the thermodynamic efficiency limits. *Nat. Nanotechnol.*, 13:920, 2018.

[7] B. Dutta, D. Majidi, N. W. Talarico, N. Lo Gullo, H. Courtois, and C. B. Winkelmann. Single-Quantum-Dot Heat Valve. *Phys. Rev. Lett.*, 125:237701, Dec 2020.

[8] Samuel Häusler, Philipp Fabritius, Jeffrey Mohan, Martin Lebrat, Laura Corman, and Tilman Esslinger. Interaction-assisted reversal of thermopower with ultra-cold atoms. *Phys. Rev. X*, 11:021034, May 2021.

[9] Luigi Amico, Dana Anderson, Malcolm Boshier, Jean-Philippe Brantut, Leong-Chuan Kwek, Anna Minguzzi, and Wolf von Klitzing. Atomtronic circuits: from many-body physics to quantum technologies. *arXiv:2107.08561v2*, 2022.

[10] A. Ronzani, B. Karimi, J. Senior, Y.-C. Chang, J.T. Peltonen, C. Chen, and J.P. Pekola. Tunable photonic heat transport in a quantum heat valve. *Nat. Phys.*, 14:991, 2018.

[11] O. Maillet, D. Subero, J.T. Peltonen, D.S. Golubev, and J.P. Pekola. Electric field control of radiative heat transfer in a superconducting circuit. *Nat. Commun.*, 11:1, 2020.

[12] Marlon Brenes, Juan José Mendoza-Arenas, Archak Purkayastha, Mark T. Mitchison, Stephen R. Clark, and John Goold. Tensor-network method to simulate strongly interacting quantum thermal machines. *Phys. Rev. X*, 10:031040, Aug 2020.

[13] Shishir Khandelwal, Nicolas Brunner, and Géraldine Haack. Signatures of Liouvillian Exceptional Points in a Quantum Thermal Machine. *PRX Quantum*, 2:040346, Dec 2021.

[14] Jonatan Bohr Brask, Fabien Clivaz, Géraldine Haack, and Armin Tavakoli. Operational nonclassicality in minimal autonomous thermal machines. *Quantum*, 6:672, March 2022.

[15] O. Marchukov, A. Volosniev, M. Valiente, D. Petrosyan, and N.T. Zinner. Quantum spin transistor with a Heisenberg spin chain. *Nat. Commun.*, 7:13070, 2016.

[16] K.W. Wilsmann, L.H. Ymai, A.P. Tonel, J. Links, and A. Foerster. Control of tunneling in an atomtronic switching device. *Commun. Phys.*, 1:91, 2018.

[17] Kasper Poulsen and Nikolaj T. Zinner. Giant magnetoresistance in boundary-driven spin chains. *Phys. Rev.*

Lett., 126:077203, Feb 2021.

[18] Kasper Poulsen, Alan C. Santos, and Nikolaj T. Zinner. Quantum Wheatstone Bridge. *Phys. Rev. Lett.*, 128:240401, Jun 2022.

[19] R. A. Pepino, J. Cooper, D. Z. Anderson, and M. J. Holland. Atomtronic circuits of diodes and transistors. *Phys. Rev. Lett.*, 103:140405, Sep 2009.

[20] Vinitha Balachandran, Giuliano Benenti, Emmanuel Pereira, Giulio Casati, and Dario Poletti. Perfect diode in quantum spin chains. *Phys. Rev. Lett.*, 120:200603, May 2018.

[21] Vinitha Balachandran, Stephen R. Clark, John Goold, and Dario Poletti. Energy current rectification and mobility edges. *Phys. Rev. Lett.*, 123:020603, Jul 2019.

[22] Emmanuel Pereira. Perfect thermal rectification in a many-body quantum ising model. *Phys. Rev. E*, 99:032116, Mar 2019.

[23] Vinitha Balachandran, Giuliano Benenti, Emmanuel Pereira, Giulio Casati, and Dario Poletti. Heat current rectification in segmented xxz chains. *Phys. Rev. E*, 99:032136, Mar 2019.

[24] Kazuki Yamamoto, Yuto Ashida, and Norio Kawakami. Rectification in nonequilibrium steady states of open many-body systems. *Phys. Rev. Research*, 2:043343, Dec 2020.

[25] Kang Hao Lee, Vinitha Balachandran, Ryan Tan, Chu Guo, and Dario Poletti. Giant spin current rectification due to the interplay of negative differential conductance and a non-uniform magnetic field. *Entropy*, 22(11), 2020.

[26] Kang Hao Lee, Vinitha Balachandran, and Dario Poletti. Giant rectification in segmented, strongly interacting spin chains despite the presence of perturbations. *Phys. Rev. E*, 103:052143, May 2021.

[27] Kang Hao Lee, Vinitha Balachandran, Chu Guo, and Dario Poletti. Transport and spectral properties of the $xx + xxz$ diode and stability to dephasing. *Phys. Rev. E*, 105:024120, Feb 2022.

[28] Kasper Poulsen, Alan C. Santos, Lasse B. Kristensen, and Nikolaj T. Zinner. Entanglement-enhanced quantum rectification. *Phys. Rev. A*, 105:052605, May 2022.

[29] Alessandra Chioquetta, Emmanuel Pereira, Gabriel T. Landi, and Raphael C. Drumond. Rectification induced by geometry in two-dimensional quantum spin lattices. *Phys. Rev. E*, 103:032108, Mar 2021.

[30] Vipul Upadhyay, M. Tahir Naseem, Rahul Marathe, and Özgür E. Müstecaplıoğlu. Heat rectification by two qubits coupled with Dzyaloshinskii-Moriya interaction. *Phys. Rev. E*, 104:054137, Nov 2021.

[31] M. Schulz, C. A. Hooley, R. Moessner, and F. Pollmann. Stark many-body localization. *Phys. Rev. Lett.*, 122:040606, Jan 2019.

[32] Evert van. Nieuwenburg, Yuval Baum, and Gil Refael. From Bloch oscillations to many-body localization in clean interacting systems. *Proc. Natl. Acad. Sci. U.S.A.*, 116:9269, 2019.

[33] S. R. Taylor, M. Schulz, F. Pollmann, and R. Moessner. Experimental probes of Stark many-body localization. *Phys. Rev. B*, 102:054206, Aug 2020.

[34] Ruixiao Yao, Titas Chanda, and Jakub Zakrzewski. Many-body localization in tilted and harmonic potentials. *Phys. Rev. B*, 104:014201, Jul 2021.

[35] Guy Zisling, Dante M. Kennes, and Yevgeny Bar Lev. Transport in Stark many-body localized systems. *Phys.*

Rev. B, 105:L140201, Apr 2022.

[36] Vedika Khemani, Michael Hermele, and Rahul Nandkishore. Localization from Hilbert space shattering: From theory to physical realizations. *Phys. Rev. B*, 101:174204, May 2020.

[37] Jean-Yves Desaules, Ana Hudomal, Christopher J. Turner, and Zlatko Papić. Proposal for Realizing Quantum Scars in the Tilted 1D Fermi-Hubbard Model. *Phys. Rev. Lett.*, 126:210601, May 2021.

[38] A. Kshetrimayum, J. Eisert, and D. M. Kennes. Stark time crystals: Symmetry breaking in space and time. *Phys. Rev. B*, 102:195116, Nov 2020.

[39] C. Klöckner, C. Karrasch, and D. M. Kennes. Nonequilibrium Properties of Berezinskii-Kosterlitz-Thouless Phase Transitions. *Phys. Rev. Lett.*, 125:147601, Oct 2020.

[40] W. Morong, F. Liu, P. Becker, K.S. Collins, L. Feng, A. Kyprianidis, G. Pagano, T. You, A.V. Gorshkov, and C. Monroe. Observation of Stark many-body localization without disorder. *Nature*, 599:393, 2021.

[41] Elmer Guardado-Sanchez, Alan Morningstar, Benjamin M. Spar, Peter T. Brown, David A. Huse, and Waseem S. Bakr. Subdiffusion and Heat Transport in a Tilted Two-Dimensional Fermi-Hubbard System. *Phys. Rev. X*, 10:011042, Feb 2020.

[42] Sebastian Scherg, Thomas Kohlert, Pablo Sala, Frank Pollmann, Bharath Hebbe Madhusudhana, Immanuel Bloch, and Monika Aidelsburger. Observing nonergodicity due to kinetic constraints in tilted Fermi-Hubbard chains. *Nat. Commun.*, 12:4490, 2021.

[43] Bharath Hebbe Madhusudhana, Sebastian Scherg, Thomas Kohlert, Immanuel Bloch, and Monika Aidelsburger. Benchmarking a Novel Efficient Numerical Method for Localized 1D Fermi-Hubbard Systems on a Quantum Simulator. *PRX Quantum*, 2:040325, Nov 2021.

[44] Qiujiang Guo, Chen Cheng, Hekang Li, Shibo Xu, Pengfei Zhang, Zhen Wang, Chao Song, Wuxin Liu, Wenhui Ren, Hang Dong, Rubem Mondaini, and H. Wang. Stark Many-Body Localization on a Superconducting Quantum Processor. *Phys. Rev. Lett.*, 127:240502, Dec 2021.

[45] Elmer V. H. Doggen, Igor V. Gornyi, and Dmitry G. Polyakov. Stark many-body localization: Evidence for Hilbert-space shattering. *Phys. Rev. B*, 103:L100202, Mar 2021.

[46] Gregory H. Wannier. Dynamics of band electrons in electric and magnetic fields. *Rev. Mod. Phys.*, 34:645–655, Oct 1962.

[47] Mark T. Mitchison and Martin B. Plenio. Non-additive dissipation in open quantum networks out of equilibrium. *New J. Phys.*, 20(3):033005, mar 2018.

[48] Heinz-Peter Breuer and Francesco Petruccione. *The Theory of Open Quantum Systems*. Oxford University Press, 2007.

[49] G. Benenti, G. Casati, T. Prosen, D. Rossini, and M. Žnidarič. Charge and spin transport in strongly correlated one-dimensional quantum systems driven far from equilibrium. *Phys. Rev. B*, 80:35110, 2009.

[50] J. J. Mendoza-Arenas, T. Grujic, D. Jaksch, and S. R. Clark. Dephasing enhanced transport in nonequilibrium strongly correlated quantum systems. *Phys. Rev. B*, 87:235130, Jun 2013.

[51] Marko Žnidarič. Solvable quantum nonequilibrium model exhibiting a phase transition and a matrix product rep-

resentation. *Phys. Rev. E*, 83:011108, Jan 2011.

[52] J. J. Mendoza-Arenas, S. Al-Assam, S. R. Clark, and D. Jaksch. Heat transport in an XXZ spin chain: from ballistic to diffusive regimes and dephasing enhancement. *J. Stat. Mech. Theory Exp.*, 2013:P07007, 2013.

[53] Saulo H.S. Silva, Gabriel T. Landi, and Emmanuel Pereira. Non-trivial effect of dephasing: Enhancement of rectification of spin current in graded xx chains. *arXiv:2207.02693v2*, 2022.

[54] L. D. Landau and E. M. Lifshitz. *Quantum Mechanics: Non-Relativistic Theory*, volume 3. Butterworth-Heinemann, Amsterdam, 2005. Secs. 79 and 96.

[55] Marek M. Rams and Michael Zwolak. Breaking the Entanglement Barrier: Tensor Network Simulation of Quantum Transport. *Phys. Rev. Lett.*, 124:137701, Mar 2020.

[56] Gerald E. Fux, Eoin P. Butler, Paul R. Eastham, Brendon W. Lovett, and Jonathan Keeling. Efficient Exploration of Hamiltonian Parameter Space for Optimal Control of Non-Markovian Open Quantum Systems. *Phys. Rev. Lett.*, 126:200401, May 2021.

[57] Andreu Riera-Campeny, Anna Sanpera, and Philipp Strasberg. Quantum Systems Correlated with a Finite Bath: Nonequilibrium Dynamics and Thermodynamics. *PRX Quantum*, 2:010340, Mar 2021.

[58] Sebastian Krinner, Tilman Esslinger, and Jean-Philippe Brantut. Two-terminal transport measurements with cold atoms. *Journal of Physics: Condensed Matter*, 29(34):343003, jul 2017.

[59] Ruichao Ma, Brendan Saxberg, Clai Owens, Nelson Leung, Yao Lu, Jonathan Simon, and David I. Schuster. A dissipatively stabilized Mott insulator of photons. *Nature*, 566:51, 2019.

[60] Marko Žnidarič. Exact solution for a diffusive nonequilibrium steady state of an open quantum chain. *J. Stat. Mech.*, 2010(05):L05002, may 2010.

[61] Tomaz Prosen and Marko Žnidarič. Matrix product simulations of non-equilibrium steady states of quantum spin chains. *J. Stat. Mech. Theory Exp.*, 2009(02):P02035, 2009.

[62] Michael Zwolak and Guifré Vidal. Mixed-state dynamics in one-dimensional quantum lattice systems: A time-dependent superoperator renormalization algorithm. *Phys. Rev. Lett.*, 93:207205, Nov 2004.

[63] F. Verstraete, J. J. García-Ripoll, and J. I. Cirac. Matrix product density operators: Simulation of finite-temperature and dissipative systems. *Phys. Rev. Lett.*, 93:207204, Nov 2004.

[64] S. Al-Assam, S. R. Clark, D. Jaksch, and TNT Development Team. Tensor Network Theory Library, Beta Version 1.2.0, 2016.

[65] S. Al-Assam, S. R. Clark, and D. Jaksch. The Tensor Network Theory Library. *J. Stat. Mech.*, 2017:093102, 2017.

[66] Jung-Hoon Jung and Jae Dong Noh. Guide to Exact Diagonalization Study of Quantum Thermalization. *J. Korean Phys. Soc.*, 76:670, 2020.

AUTHOR CONTRIBUTIONS

J.J.M.A. proposed the rectification scheme and performed the numerical and analytical calculations, under the supervision of S.R.C.. J.J.M.A and S.R.C. analyzed and discussed the results and the explanation of the phenomenon, and contributed to writing the manuscript.

COMPETING INTERESTS

The authors declare no competing interests.

SUPPLEMENTARY METHODS

Exact solution of noninteracting systems

Here we provide details of the NESS solution for tilted systems with $\Delta = 0$, arbitrary Γ and f, sketched in Fig. 5, using the Ansatz (5) of the main text. As discussed in Methods, due to the symmetric boundary driving several coefficients of this Ansatz are zero or equal to others. Assuming N even, the symmetry relations are

$$a_k = -a_{N-k+1}, \qquad k = 1, \ldots, \frac{N}{2} \qquad (9)$$

for the populations and

$$h_k^{(l)} = (-1)^l h_{N-l-k+2}^{(l)}, \qquad b_k^{(l)} = (-1)^l b_{N-l-k+2}^{(l)} \quad (10)$$

with $k = 1, \ldots \frac{N-2l'}{2} + 1$, and where $l = 2l'$ for l even and $l = 2l' - 1$ for l odd. If N is odd the central population vanishes, namely $a_{\frac{N+1}{2}} = 0$, the recursions for $h_k^{(l)}$ and $b_k^{(l)}$ hold but for $k = 1, \ldots \frac{N-2l'+1}{2}$, and

$$h_{\frac{N-l}{2}+1}^{(l)} = b_{\frac{N-l}{2}+1}^{(l)} = 0 \text{ for } l \text{ odd.} \qquad (11)$$

Thus with N even we have $\frac{N^2}{2} + 1$ unknown coefficients, while for N odd we have $\frac{(N-1)^2}{2} + 1$ unknown coefficients and N zero coefficients. This indicates that the same effort is required to solve systems of $N = 2M$ and $N = 2M + 1$ sites.

Considering these symmetries, we obtain the following set of equations after inserting the Ansatz in the master equation and grouping the coefficients of each resulting operator. From the coefficients in front of $2n_1 - 1$ we get

$$a_1 + \frac{4b^{(2)}}{\Gamma} = f. \qquad (12)$$

From the coefficients in front of $B_k^{(2)}$ ($k = 1, \ldots, \frac{N}{2} - 1$) we have

$$-\frac{\Gamma}{2} b^{(2)} \delta_{k,1} + 2J(a_k - a_{k+1}) \\ + 2J\left(h_{k-1}^{(3)} - h_k^{(3)}\right) - 2Eh_k^{(2)} = 0. \qquad (13)$$

This equation is modified for $k = \frac{N}{2}$ (i.e. when reaching the center of the system), since $a_{\frac{N}{2}} = -a_{\frac{N}{2}+1}$ and $h_{\frac{N}{2}}^{(3)} = -h_{\frac{N}{2}-1}^{(3)}$. Thus here we have

$$2Ja_{\frac{N}{2}} + 2Jh_{\frac{N}{2}-1}^{(3)} - Eh_{\frac{N}{2}}^{(2)} = 0. \qquad (14)$$

From the coefficients in front of $H_k^{(2)}$ ($k = 1, \ldots, \frac{N}{2} - 1$) we have

$$-\frac{\Gamma}{2} h_1^{(2)} \delta_{k,1} + 2J\left(b_k^{(3)} - b_{k-1}^{(3)}\right) + 2Eb^{(2)} = 0, \qquad (15)$$

which changes for $k = \frac{N}{2}$ since $b_{\frac{N}{2}}^{(3)} = -b_{\frac{N}{2}-1}^{(3)}$, giving

$$-4Jb_{\frac{N}{2}-1}^{(3)} + 2Eb^{(2)} = 0. \qquad (16)$$

For $l \geq 3$ even, from the coefficients in front of $B_k^{(l)}$ ($k = 1, \ldots, \frac{N-l}{2}$), we get

$$-\frac{\Gamma}{2} b_1^{(l)} \delta_{k,1} (1 + \delta_{lN}) + 2J\left(h_{k+1}^{(l-1)} - h_k^{(l-1)}\right) \\ + 2J\left(h_{k-1}^{(l+1)} - h_k^{(l+1)}\right) - 2(l-1)Eh_k^{(l)} = 0, \qquad (17)$$

and from the coefficients in front of $H_k^{(l)}$ we have

$$-\frac{\Gamma}{2} h_1^{(l)} \delta_{k,1} (1 + \delta_{lN}) + 2J\left(b_k^{(l-1)} - b_{k+1}^{(l-1)}\right) \\ + 2J\left(b_k^{(l+1)} - b_{k-1}^{(l+1)}\right) + 2(l-1)Eb_k^{(l)} = 0, \qquad (18)$$

where the δ_{lN} results because for the last l the driving terms of both boundaries are equal and thus are summed. For $k = \frac{N-l}{2} + 1$, the corresponding equations are

$$-2Jh_{\frac{N-l}{2}+1}^{(l-1)} + 2Jh_{\frac{N-l}{2}}^{(l+1)} - (l-1)Eh_{\frac{N-l}{2}+1}^{(l)} = 0 \quad (19)$$

$$2Jb_{\frac{N-l}{2}+1}^{(l-1)} - 2Jb_{\frac{N-l}{2}}^{(l+1)} + (l-1)Eb_{\frac{N-l}{2}+1}^{(l)} = 0. \quad (20)$$

Finally, for $l \geq 3$ odd, the same relations hold for $k = 1, \ldots, \frac{N-l+1}{2}$. This completes the set of $\frac{N^2}{2} + 1$ linear equations for N even and of $\frac{(N-1)^2}{2} + 1$ equations for N odd, which can be solved exactly for hundreds of sites with standard linear algebra packages and a moderate computational effort.

Importantly, if $E = 0$, this problem reduces to that of a noninteracting ballistic conductor [51, 60]. Here the equations for coefficients in front of $H_k^{(2)}$, $H_k^{(l)}$ and $B_k^{(l)}$ for $l \geq 3$ decouple from the rest, and form a set of homogeneous equations with the same number on unknowns; the solution of this system is the trivial one where the corresponding coefficients $h_k^{(2)}$, $h_k^{(l)}$ and $b_k^{(l)}$ are zero. This leads to the size-independent particle current

$$\mathcal{J} = \frac{2\Gamma f}{\Gamma^2 + 16}, \qquad (21)$$

and a flat population profile in the bulk, as seen from Eq. (13). In addition, if $E \neq 0$ but $f = 0$, the full system
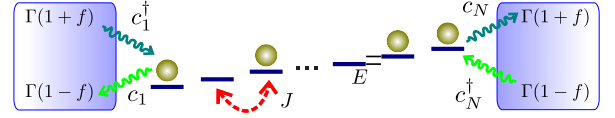

FIG. 5. Nonequilibrium noninteracting lattice of spinless fermions, with hopping J and tilt $E > 0$. The system is taken out of equilibrium by injection and ejection of particles at the boundaries, with imbalance f between both processes and coupling Γ to both reservoirs.

of equations is homogeneous, where only the trivial solution of all parameters being zero is possible. This corresponds to the NESS being equal to the identity (infinite temperature state), as expected.

Ansatz for domain NESS
To unravel the structure of the insulating domain reverse-driving NESSs, consider first $J = 0$, where the Hamiltonian eigenstates are products in the Fock basis. The highest energy of the n particle sector corresponds to a single eigenstate with a domain on the right (only degenerate with the domain on the left when $E = 0$), denoted as $|B_n\rangle = |00\ldots0_{N-n}11\ldots1_n\rangle$. Crucially, this state increases its separation in energy from the rest as E or Δ increase, and is a dark configuration of the $f = -1$ driving [50]. For low hopping $J \ll \Delta$ or E and right-to-left particle transport, the associated eigenstate $|\Psi_n^D\rangle$ is perturbatively built from break-away configurations corresponding to the most inner particle moving to the left and the most inner hole to the right. These are denoted as $|\psi_k^n\rangle_p$ and $|\psi_k^n\rangle_h$ respectively for k hopping processes. Due to the energy gap $\Delta + \frac{k}{2}E$ between $|B_n\rangle$ and these configurations, the kth order correction to $|B_n\rangle$ in perturbation theory is $\sim |\psi_k^n\rangle_h + |\psi_k^n\rangle_p$ with amplitude

$$d_k = \frac{J^k}{(2\Delta + E)(2\Delta + 2E)\cdots(2\Delta + kE)}$$
$$= \frac{f_j}{\left(\frac{2\Delta}{E} + 1\right)^{(k)}}\left(\frac{J}{E}\right)^k. \quad (22)$$

Here we introduced the Pochhammer symbol $y^{(k)} = y(y+1)(y+2)\cdots(y+k-1) = \Gamma(y+k)/\Gamma(y)$, and a factor f_j different from 1 when the particle (hole) reaches site $j = 1$ ($j = N$):

$$f_j = \begin{cases} \frac{2\Delta+(N-n)E}{\Delta+(N-n)E} & \text{if} \quad j = 1 \\ \frac{2\Delta+nE}{\Delta+nE} & \text{if} \quad j = N \\ 1 & \text{otherwise.} \end{cases} \quad (23)$$

In the noninteracting ($\Delta = 0$) and homogeneous ($E = 0$) limits the amplitude reduces to

$$d_k = \begin{cases} \frac{1}{k!}\left(\frac{J}{E}\right)^k = \frac{1}{k!}e^{-k/\xi(E)} & \text{if} \quad \Delta = 0 \\ \left(\frac{J}{2\Delta}\right)^k = e^{-k/\xi(2\Delta)} & \text{if} \quad E = 0, \end{cases} \quad (24)$$

with localization length scale $\xi(Q) = 1/\ln(Q/J)$. Thus, in general the corrections to $|B_n\rangle$ are suppressed at least exponentially with k. In addition, since only the configurations with a particle on site 1 or a hole on site N are not dark (i.e. they are affected by the $f = -1$ driving), $|\Psi_n^D\rangle$ become exponentially close to being dark states of the $f = -1$ driving. Note that an identical description can be performed in the forward $f = 1$ driving scheme for the homogeneous interacting case (with degenerate left and right high-energy domains) and the noninteracting tilted system (where the left domain is the state of lowest energy). However, when interactions and tilt coexist this approach is no longer valid.

From the dark states $|\Psi_n^D\rangle$ we define the statistical mixture

$$\rho_{\text{Dom}} = \sum_{n=0}^N p_n|\Psi_D(n)\rangle\langle\Psi_D(n)|, \qquad \sum_{n=0}^N p_n = 1, \quad (25)$$

where the probabilities p_n are determined from a detailed balance condition. Namely, if $P_{n\to m}$ is the transition probability from particle number sector n to sector m due to the driving, the detailed balance condition is $P_{n\to n+1} + P_{n\to n-1} = P_{n-1\to n} + P_{n+1\to n}$, with probabilities

$$P_{n\to n+1} = p_n\Gamma\langle\Psi_D(n)|\sigma_1^-\sigma_1^+|\Psi_D(n)\rangle$$
$$P_{n\to n-1} = p_n\Gamma\langle\Psi_D(n)|\sigma_N^+\sigma_N^-|\Psi_D(n)\rangle. \quad (26)$$

The solution of these equations for an even system gives

$$p_{\frac{N}{2}+m} = \frac{p}{\prod_{j=-|m|+1}^{|m|-1}\left(\frac{2\Delta}{E} + \frac{N}{2} + j\right)^{2(|m|-|j|)}}\left(\frac{J}{E}\right)^{2|m|^2} \quad (27)$$

for $-N/2 \le m \le N/2$. Note that this distribution of probabilities is symmetric, so $p_{\frac{N}{2}+m} = p_{\frac{N}{2}-m}$. Here $p = p_{\frac{N}{2}}$ is fixed by the normalization condition in Eq. (8), and also is the highest of all the probabilities p_n. Thus, the NESS of the system is largely dominated by the state with occupied and empty domains of equal size.

Implementation of CP symmetric Hamiltonian
To illustrate how the exact eigenstructure of the CP symmetric tilted Hamiltonian is obtained, we take $N = 4$. We initially consider the half-filling sector, where the particle number operator $\tilde{N}$ and CP symmetry operator U commute. First we identify each equivalent class (EC), corresponding to each set of basis states that are equivalent under CP symmetry, and their representative state (RS) [66]. These are given in table I, along with the period of each EC.

The basis elements of the even CP half-filled sector,

RS	EC	Period
1001	1001	2
	0110	
1100	1100	1
1010	1010	1
0101	0101	1
0011	0011	1

TABLE I. Representative states for $N = 4$ half-filled system, states of the corresponding equivalent class and period.

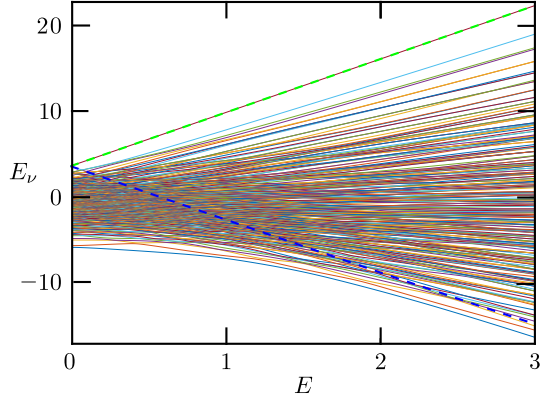which are common eigenstates of the number and CP

FIG. 6. Eigenstructure of half-filled even CP symmetric sector for $N = 10$ and $\Delta = 2$. The solid lines correspond to the eigenenergies, and the dashed lines to the second-order perturbative corrections to the domains states pinned to the right (green) and left (blue) boundaries, namely Eqs. (34).

symmetry operator, are thus

$$
\begin{aligned}
|1001, +\rangle &= \frac{1}{\sqrt{2}}(|1001\rangle + |0110\rangle) \\
|1100, +\rangle &= |1100\rangle, \ |1010, +\rangle = |1010\rangle, \\
|0101, +\rangle &= |0101\rangle, \ |0011, +\rangle = |0011\rangle.
\end{aligned}
\tag{28}
$$

The Hamiltonian of this symmetry sector, with the given order of basis elements, is

$$
H^{2e} = \frac{1}{4}
\begin{pmatrix}
-\Delta & 0 & 2\sqrt{2}J & 2\sqrt{2}J & 0 \\
0 & \Delta + 4E & 2J & 0 & 0 \\
2\sqrt{2}J & 2J & -3\Delta + 2E & 0 & 0 \\
2\sqrt{2}J & 0 & 0 & -3\Delta - 2E & 2J \\
0 & 0 & 0 & 2J & \Delta - 4E
\end{pmatrix}.
\tag{29}
$$

Its spectrum is depicted in Fig. 3a of the main text; due to the no-crossing theorem [54], it only shows avoided crossings. On the other hand, the half-filled odd CP symmetric sector only has one basis element, namely

$$
|1001, -\rangle = \frac{1}{\sqrt{2}}(|1001\rangle - |0110\rangle),
\tag{30}
$$

with energy $-\Delta/4$. This completes the 6 states of the half-filling sector.

Beyond half filling the CP symmetry operator does not commute with $\tilde{N}$. Thus we can build sectors of fixed number of particles or fixed symmetry, but not both. However, each case has redundant information. In the former scenario, the Hamiltonian of m particles is equal to that of m holes. In the latter, the Hamiltonians of even and odd CP symmetric sectors are also identical. To see this, note that the basis elements of each sector are the $\pm$ equal superpositions of the states of each EC

RS	EC	Period
1111	1111 0000	2
1110	1110 1000	2
1101	1101 0100	2
1011	1011 0010	2
0111	0111 0001	2

TABLE II. Representative states for $N = 4$ beyond half filling, states of the corresponding equivalent class and period.

listed in table II, namely

$$
\begin{aligned}
|1111, \pm\rangle &= \frac{1}{\sqrt{2}}(|1111\rangle \pm |0000\rangle) \\
|1110, \pm\rangle &= \frac{1}{\sqrt{2}}(|1110\rangle \pm |1000\rangle) \\
|1101, \pm\rangle &= \frac{1}{\sqrt{2}}(|1101\rangle \pm |0100\rangle) \\
|1011, \pm\rangle &= \frac{1}{\sqrt{2}}(|1011\rangle \pm |0010\rangle) \\
|0111, \pm\rangle &= \frac{1}{\sqrt{2}}(|0111\rangle \pm |0001\rangle).
\end{aligned}
\tag{31}
$$

The $\pm$ superposition states of 0 and 4 particles are disconnected from the other basis elements, and have energy $3\Delta/4$. The states of 1 and 3 particles are connected with each other by the Hamiltonian, which has the matrix representation

$$
H^{e/o} = \frac{1}{4}
\begin{pmatrix}
\Delta + 3E & 2J & 0 & 0 \\
2J & -\Delta + E & 2J & 0 \\
0 & 2J & -\Delta - E & 2J \\
0 & 0 & 2J & \Delta - 3E
\end{pmatrix}.
\tag{32}
$$

Similarly to the half-filled case, the spectrum of this Hamiltonian features avoided crossings only. This completes the 10 states of the sectors beyond half filling, and thus the 16 states of the $N = 4$ system.

The above construction can be directly extended to larger systems. This is exemplified in Fig. 6 for the even CP symmetry sector of 10 sites, which corresponds to results presented in Fig. 4d-f of the main text.

Perturbative calculation of eigenenergies
Given the many-body nature of our problem, it is not feasible to obtain exactly the eigenstructure of the Hamiltonian for large systems, even with the explicit use of the CP symmetry described in the previous subsection. Considering that our giant rectification mechanism manifests
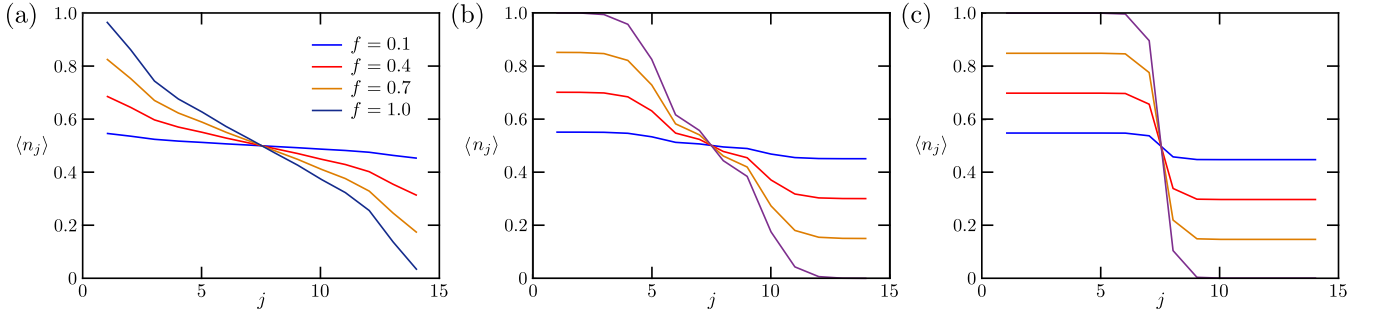
FIG. 7. Population profiles for noninteracting lattices with $N = 14$, different tilts E and driving parameters f. **a** $E = 0.3$. **b** $E = 0.6$. **c** $E = 3.0$.

for strong interactions, we perform a perturbative calculation of the most important eigenstates in this limit. For this we consider first the case of zero hopping, where the eigenstates are product states in the Fock basis. Here, the energies for N sites and domains of n particles pinned to the left (L) and right (R) boundaries are

$$E_{n,\mathrm{L}} = \frac{1}{4}\left[\Delta(N - 3) - En(N - n)\right],$$
$$E_{n,\mathrm{R}} = \frac{1}{4}\left[\Delta(N - 3) + En(N - n)\right]. \tag{33}$$

Clearly both states are degenerate and have the highest energy of the n particle sector in the absence of tilt [50]. For a finite tilt, $E_{n,\mathrm{R}}$ is the highest eigenstate of the n particle sector, while $E_{n,\mathrm{L}}$ is the second highest one for low E and the lowest one for very large E.

When turning on a very weak hopping J, these energies are corrected by second-order processes of the most inner particle jumping to the neighboring empty site and then jumping back. Assuming no degenerate states, the corrected energies are

$$\tilde{E}_{n,\mathrm{L}} = E_{n,\mathrm{L}} + \frac{J^2}{4\Delta - 2E},$$
$$\tilde{E}_{n,\mathrm{R}} = E_{n,\mathrm{R}} + \frac{J^2}{4\Delta + 2E}. \tag{34}$$

For $N = 4$, we identify $\tilde{E}_{2,\mathrm{R}} = \tilde{E}_{0011}$ as the energy $\nu = 5$ of the half-filled even CP eigenstructure of Fig. 3a of the main text, which monotonically increases with E. Also, far from $E = 2\Delta$, $\tilde{E}_{2,\mathrm{L}} = \tilde{E}_{1100}$ corresponds to the eigenenergy whose avoided crossings in the exact spectrum match the forward transport resonances, namely to $\nu = 4$ for $0 \leq E \lesssim 2$, $\nu = 3$ for $2 \lesssim E \lesssim 4$, $\nu = 2$ for $4 \lesssim E \lesssim 8$ and $\nu = 1$ for $E \gg 1$. Similarly, in Fig. 6 we plot $\tilde{E}_{5,\mathrm{R}}$ and $\tilde{E}_{5,\mathrm{L}}$ for $N = 10$ sites, indicated by green and blue dashed lines respectively.

We also focus on the case of $L = 4$ to perturbatively calculate the other energies associated to the basis elements of the half-filled even CP symmetry sector. In the

zero hopping limit, these are

$$E_{1010} = E_{\nu=1} = -\frac{1}{4}(2E + 3\Delta),$$
$$E_{0101} = E_{\nu=2} = \frac{1}{4}(2E - 3\Delta), \tag{35}$$
$$E_{1001,+} = E_{\nu=3} = -\frac{\Delta}{4}.$$

Turning on a weak hopping, and keeping up to $\mathcal{O}(J^2)$, the corrected energies are

$$\tilde{E}_{1010} = E_{1010} + \frac{J^2}{2}\left[\frac{1}{E - 2\Delta} - \frac{2}{E + \Delta}\right],$$
$$\tilde{E}_{0101} = E_{0101} + \frac{J^2}{2}\left[\frac{2}{E - \Delta} - \frac{1}{E + 2\Delta}\right], \tag{36}$$
$$\tilde{E}_{1001,+} = E_{1001,+} + J^2\left[\frac{1}{\Delta + E} + \frac{1}{\Delta - E}\right].$$

For tilts lower than those of the divergences ($E = \Delta, 2\Delta$), these expressions work reasonably well, as seen in Fig. 3a of the main text. In fact, the first crossing of $\tilde{E}_{1100}$ and $\tilde{E}_{1001,+}$ takes place at $E \approx 2.08$, which is very close to the location of the first forward current resonance, $E = 2.15$.

SUPPLEMENTARY DISCUSSION

Analytical results for small noninteracting chains
Now we provide analytical results for the exact set of linear equations of $\Delta = 0$, focusing on the particle current and population profile for small lattices. We take first $N = 4$, which corresponds to a set of 9 equations and 9 unknowns, namely $a_1, a_2, b^{(2)}, h_1^{(2)}, h_2^{(2)}, b_1^{(3)}, h_1^{(3)}, b_1^{(4)}$ and $h_1^{(4)}$. Even though this system can be easily solved, it leads to cumbersome expressions for the transport properties. Thus we consider two limits. First, for $E \ll 1$ the particle current to lowest order in E is given by

$$\mathcal{J} = \frac{2\Gamma f}{\Gamma^2 + 16} - \frac{1}{2}E^2\Gamma f\frac{(160 + \Gamma^2)}{(16 + \Gamma^2)^2}. \tag{37}$$
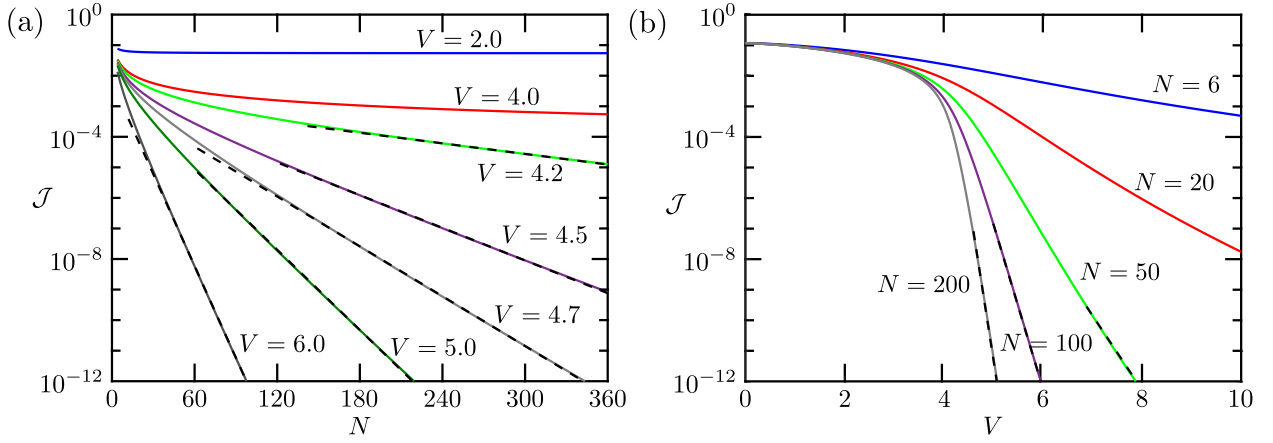
FIG. 8. Particle current in noninteracting tilted lattices. **a** As a function of N for different values of V. The dashed lines correspond to fits to exponential functions $\sim e^{-cN}$, with exponents $c = 0.0133(1), 0.0410(2), 0.0626(2), 0.101(1), 0.231(1)$ for $V = 4.2, 4.5, 4.7, 5.0, 6.0$ respectively. **b** As a function of V for different values of N. The dashed lines correspond to fits to exponential functions $\sim e^{-dV}$, with exponents $d = 5.60(5), 12.42(6), 24.1(3)$ for $N = 50, 100, 200$ respectively.

Thus the current decreases quadratically from the $E = 0$ result of Eq. (21). A more interesting situation is that of very large tilt $E \gg 1$. Here we get the current

$$\mathcal{J} = \frac{1}{8}\Gamma f E^{-4} \qquad (38)$$

and the coefficients

$$a_1 = f(1 - E^{-4}), \qquad a_2 = f\left(1 - \frac{5}{2}E^{-2}\right), \qquad (39)$$

with $a_3 = -a_2$ and $a_4 = -a_1$. This indicates that a large tilt leads to an insulating state. The current is suppressed as a power law of E, as well as the deviations of the populations from $(1 + f)/2$ and $(1 - f)/2$ on the left and right halves of the chain, respectively. Indeed, if $f = 1$, as in our numerical calculations, the populations $\langle n_k \rangle = (a_k + 1)/2$ of the chain are

$$
\langle n_1 \rangle = 1 - \frac{1}{2}E^{-4}, \qquad \langle n_2 \rangle = 1 - \frac{5}{4}E^{-2},
$$
$$
\langle n_3 \rangle = \frac{5}{4}E^{-2}, \qquad \langle n_4 \rangle = \frac{1}{2}E^{-4}. \qquad (40)
$$

This corresponds to the formation of almost fully-occupied and empty domains on the left and right halves of the system respectively. If $f < 1$ the system is also insulating, with domains of population values closer to $1/2$, as shown in Fig. 7 for larger systems.

Crucially, the $f = 1$ population results are reproduced with the insulating Ansatz of Eq. (8). For instance, for any even $N \geq 4$ and keeping only $m = \pm 1$ in Eq. (27), the probabilities of the Ansatz are up to $\mathcal{O}(E^{-2})$

$$p_{\frac{N}{2}} = 1 - 8\left(\frac{J}{EN}\right)^2, \qquad p_{\frac{N}{2}\pm 1} = 4\left(\frac{J}{EN}\right)^2. \qquad (41)$$

This leads to the general expression

$$\left\langle n_{\frac{N}{2}} \right\rangle = 1 - \left(\frac{J}{E}\right)^2\left[1 + \left(\frac{2}{N}\right)^2\right], \qquad (42)$$

which agrees with the result of $\langle n_2 \rangle$ of Eq. (40) for $N = 4$. We have also reproduced $\langle n_1 \rangle$ keeping up to $\mathcal{O}(E^{-4})$. This provides a benchmark of the Ansatz of Eq. (8). In addition, we calculated the exact solution of the linear set of equations for $N = 5$, which has the same number of unknowns. In the limit of low tilt $E \ll 1$, we get

$$\mathcal{J}^{\mathrm{S}} = \frac{2\Gamma f}{\Gamma^2 + 16} - 2E^2\Gamma f\frac{(80 + \Gamma^2)}{(16 + \Gamma^2)^2}. \qquad (43)$$

It has a very similar form to that of $N = 4$, but with larger deviation from the ballistic result. On the other hand, in the limit $E \gg 1$, we get the current

$$\mathcal{J} = \frac{1}{32}\Gamma f E^{-4} \qquad (44)$$

and $f = 1$ populations

$$
\langle n_1 \rangle = 1 - \frac{1}{8}E^{-4}, \qquad \langle n_2 \rangle = 1 - \frac{1}{2}E^{-2},
$$
$$
\langle n_3 \rangle = 0, \qquad \langle n_4 \rangle = \frac{1}{2}E^{-2}, \qquad \langle n_5 \rangle = \frac{1}{8}E^{-4}. \qquad (45)
$$

Thus in the large E limit the current for $N = 5$ is four times lower than that of $N = 4$, and the populations are closer to 1 on the left and to 0 on the right than those of $N = 4$. This means that even though the observables are of the same order in both sizes, the larger system favors more the formation of particle domains.

Finally, it is important to note that these results already show that there is no rectification when $\Delta = 0$, as the current is $\propto f$. Interactions are thus required in the
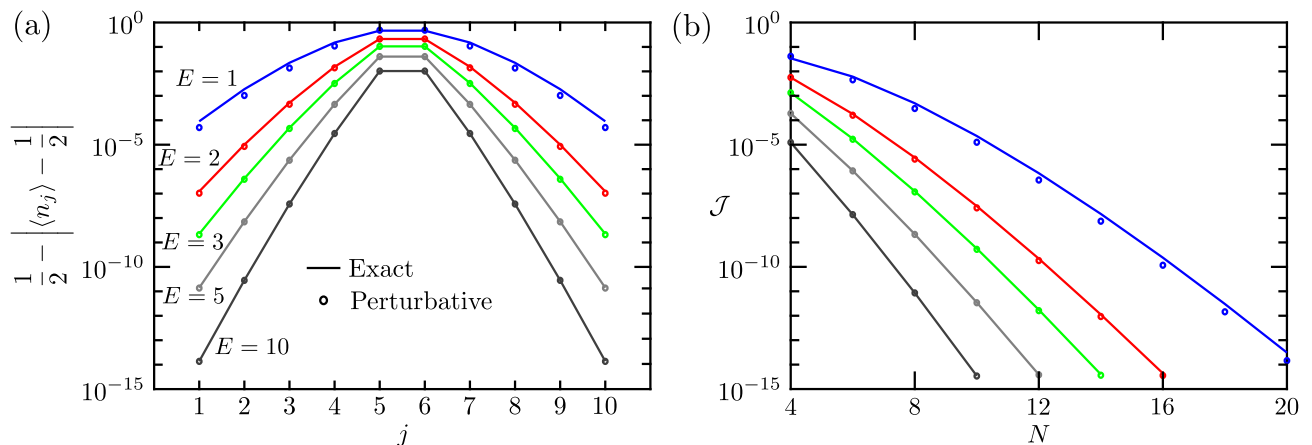
FIG. 9. Comparison of noninteracting NESS expectation values from exact calculations and insulating Ansatz. **a** Populations across a lattice of $N = 10$ and several values of E, for exact (solid lines) and perturbative ($\circ$) calculations. **b** Comparison of particle currents as a function of the system size; the same convention of panel **a** is used.

present scheme for it to behave as a diode.

Transport in noninteracting tilted lattice
Using the exact solution described in Supplementary Methods, we calculate the transport properties for noninteracting tilted systems larger than those obtained analytically in the previous section. First we consider different values of f and E on lattices of $N = 14$, as show in Fig. 7. Similarly to the results for $N = 4$ of Eq. (39), f just modifies the amplitude of the deviation of the populations from the value $1/2$, leaving the overall form of the profile identical. The effect of E (and of $V = EN$, shown in Fig. 2c of the main text) is different, as it changes the form of the profiles. Indeed, as E increases these become more flat on both halves of the lattice, preventing the propagation of particles and thus driving the system to an insulating NESS.
Furthermore, considering Eq. (12), the current is proportional to f, as in the analytical results of $N = 4, 5$. Given the latter, we analyze the current for the maximally-driven $f = 1$ case only, when varying V and N. First we evaluate $\mathcal{J}$ as a function of the system size for several values of V; the results are shown in Fig. 8a. The current decays monotonically both with V and N, as expected. Also, for large $V \gtrsim 4.5$ an exponential trend with the system size is clear, indicating insulating behavior. For lower V the decay with N is much slower, or even not appreciable in the scale of the plot (as for $V = 2$); here we anticipate that the exponential fit will emerge on length scales larger than the system size.
We also study the behavior of the current as a function of V for fixed system sizes; the results are shown in Fig. 8b. Importantly, for large-enough systems, we find an exponential decay of $\mathcal{J}$ with V from a value that decreases with N. These results evidence how rapidly an insulating state develops due to the tilt.

Accuracy of NESS insulating Ansatz
Now we show that even for small noninteracting tilted systems, the Ansatz of Eq. (8) captures very well the observed insulating behavior. For this we compare the values of the deviations of the populations from $1/2$ (Fig. 9a) and the particle currents (Fig. 9b) obtained from the Antaz and from the exact solver for a lattice of $N = 10$ sites. Remarkably, even down to $E = 1$ the results from the Ansatz are very close to the exact ones. In the presence of interactions, the comparison of both types of calculations has been given in Fig. 4 of the main text for reverse transport, again showing an excellent agreement. These results demonstrate the huge power of the Ansatz to describe the nonequilibrium properties of a boundary-driven large-domain insulating NESS.
We emphasize that in spite of the similar description of the domain-like insulating NESSs induced by interactions and tilt on their own, there are some key differences. First, the former requires a minimun value $\Delta = 1$, as for lower Δ the transport is ballistic [4, 49, 50, 52]; the latter can be achieved with any tilt provided the chain is long enough. Second, as previously discussed, insulating domains emerge for $E = 0$ and strong interactions only at $f \approx 1$, while they can do it at any f for $\Delta = 0$ and long- or tilted-enough systems.

Mechanism of forward current resonances
Some final remarks are in order regarding the mechanism underlying our quantum diode. First, such mechanism is not restricted to half filling; different particle number sectors feature avoided crossings corresponding to forward current maxima, which might even be absent from the half-filled sector. Considering this, we have accounted for every resonance reported in the main text. Second, in addition to being associated to a large coherence, a forward current resonance takes place at an avoided crossing if the corresponding current matrix ele-
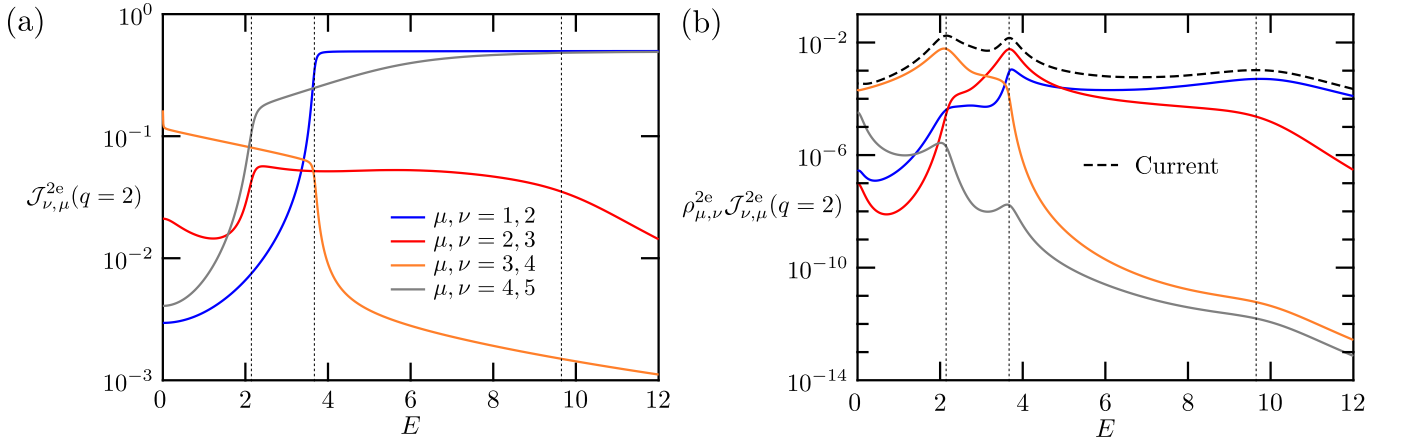
FIG. 10. Components of forward particle current in interacting tilted lattice of $N = 4$ and $\Delta = 5$. **a** Current matrix elements $\mathcal{J}^{2e}_{\nu,\mu}(q = 2)$ corresponding to the parameters of Fig. 3 of the main text. **b** Product of coherences $\rho^{2e}_{\mu,\nu}$ and matrix elements $\mathcal{J}^{2e}_{\nu,\mu}(q = 2)$, which gives contribution of the sector to the total current (dashed line).

ment $J^s_{\nu_s,\mu_s}(q)$ is significant. Otherwise, the contribution of that coherence to the current is small. This is already evidenced from the coherences shown in Fig. 3a of the main text, and the current matrix elements of Fig. 10a. The coherence between states $\mu, \nu = 3, 4$ has a large current matrix element at the tilt of the first resonance; similarly for the coherence between states $\mu, \nu = 2, 3$ at the second resonance and (in lesser way) for that between states $\mu = 1, 2$ at the third resonance. Because of

this, the product $\rho^{2e}_{\mu,\nu} \mathcal{J}^{2e}_{\nu,\mu}(q = 2)$ is large, as seen in Fig. 10b, and a resonance is clearly seen. On the other hand, even though there is a large coherence between states $\mu, \nu = 4, 5$ for $E \ll 1$, the corresponding current matrix element is strongly suppressed, leading to a barely-seen current maximum around $E \approx 0$. In conclusion, not every large coherence, arising e.g. from an avoided crossing, will correspond to a forward transport resonance.